# Dryness over the U.S. Southwest, a Springboard for Cold Season Pacific SST to Influence Warm Season Drought over the U.S. Great Plains

YIZHOU ZHUANG,[a] AMIR ERFANIAN,[a] AND RONG FU[a]

[a] *Department of Atmospheric and Oceanic Sciences, University of California, Los Angeles, Los Angeles, California*

(Manuscript received 31 January 2020, in final form 26 October 2020)

ABSTRACT: Although the influence of sea surface temperature (SST) forcing and large-scale teleconnection on summer droughts over the U.S. Great Plains has been suggested for decades, the underlying mechanisms are still not fully understood. Here we show a significant correlation between low-level moisture condition over the U.S. Southwest in spring and rainfall variability over the Great Plains in summer. Such a connection is due to the strong influence of the Southwest dryness on the zonal moisture advection to the Great Plains from spring to summer. This advection is an important contributor for the moisture deficit during spring to early summer, and so can initiate warm season drought over the Great Plains. In other words, the well-documented influence of cold season Pacific SST on the Southwest rainfall in spring, and the influence of the latter on the zonal moisture advection to the Great Plains from spring to summer, allows the Pacific climate variability in winter and spring to explain over 35% of the variance of the summer precipitation over the Great Plains, more than that can be explained by the previous documented west Pacific–North America (WPNA) teleconnection forced by tropical Pacific SST in early summer. Thus, this remote land surface feedback due to the Southwest dryness can potentially improve the predictability of summer precipitation and drought onsets over the Great Plains.

KEYWORDS: North America; Advection; Drought; Moisture/moisture budget; Seasonal forecasting

## 1. Introduction

As the world's largest exporter of grains, the United States produces nearly 40% (35%) of the global maize (soybean). Extreme summer droughts and rainy periods over the United States can trigger large disruptions in the global crop yields, international grain market, and global food security (Boyer et al. 2013; Lobell et al. 2014). Yet, we cannot predict these droughts, including the most recent extreme droughts that occurred in 2011 over the southern Great Plains and in 2012 over much of the Great Plains.

The delayed response of a regional climate to slowly varying oceanic forcing and land–atmosphere interaction provides the foundation for seasonal prediction over many regions around the world. State-of-the-art seasonal prediction models provide relatively skillful predictions of winter hydroclimate over the United States, but show virtually no skill in prediction of summer rainfall anomalies over much of the North American continent (Quan et al. 2012). Seasonal prediction of the U.S. climate becomes especially difficult in summer as the jet stream and the storm track move farther north and the precipitation regime shifts from a dominantly frontal precipitation to a tropical-like convective regime with a more regional and local character and an enhanced influence of land surface conditions (e.g., Myoung and Nielsen-Gammon 2010). Over the Great Plains, summer holds the largest share (>40%) of annual precipitation and variability of its rainfall exerts a strong control on the U.S. water resources, agriculture, and food production, as well as the global grain market and food security (Anderson et al. 2019; Boyer et al. 2013; Lobell et al. 2014). Hence, a skillful prediction of summer precipitation is central for mitigating drought impacts over this region.

Sea surface temperature anomalies (SSTA) have been considered to be a main source of predictability of anomalous precipitation over North America. Numerous studies have also suggested a significant relationship between the Great Plains summer precipitation and Pacific SSTs with two distinct modes: a tropical Pacific mode acting at shorter time scales (year-to-year) and consisting of positive correlations between the Great Plains summer rainfall and SST in the El Niño–Southern Oscillation (ENSO) region, and a North Pacific mode acting at longer time scales (multiyear to decadal) and consisting of a positive correlation between the precipitation over the Great Plains and the Pacific decadal oscillation (PDO); i.e., cold SSTA over the eastern North Pacific favor dry conditions over the Great Plains (McCabe et al. 2004; Namias 1991; Schubert et al. 2004; Wang et al. 2010; Zhao et al. 2017). The influence of Pacific SSTs on precipitation over the Great Plains is strongest when ENSO and PDO are in phase and weakest when they are out of phase (Hu and Huang 2009). Warm anomalies of the tropical Atlantic SST can also amplify the impact of a cold ENSO phase on interannual to decadal scales (e.g., Hu and Feng 2008; Mo et al. 2009; Pu et al. 2016). In addition, warmer SSTs in the North Atlantic have been shown to coincide with multiple dry indices in the long-term observed precipitation data (McCabe et al. 2004; Sutton and Hodson 2005), Palmer drought severity index (PDSI) and tree-ring proxy drought records (Feng et al. 2011), and GCM

Supplemental information related to this paper is available at the Journals Online website: https://doi.org/10.1175/JHM-D-20-0029.s1.

*Corresponding author*: Yizhou Zhuang, zhuangyz@atmos.ucla.edu

DOI: 10.1175/JHM-D-20-0029.1

simulations (Schubert et al. 2009; Seager and Hoerling 2014). In spite of the previous research strongly supporting the influence of SSTA on the summer precipitation over the Great Plains, the physical pathways behind this relationship are not yet fully understood.

The relative importance of SSTA versus internal atmospheric variability on summer precipitation over the Great Plains has remained an open question. Addressing this question is critical to skillful prediction of precipitation variability and droughts over the region. A dynamical teleconnection, through a Pacific–North American stationary wave train, has been considered to be a major atmospheric driver of the Great Plains drought onsets (Chang and Wallace 1987; Chen and Newman 1998; Lyon and Dole 1995; Namias 1991; Trenberth et al. 1988). However, during the warm season (May–August), wave propagation is generally weaker than that during the cold season. Hence, it was considered unable to explain the relation between Pacific SSTA and precipitation during the major rainy season in the Great Plains by some earlier research (Lyon and Dole 1995; Ting and Wang 1997). More recent studies have made significant progress on the time-varying influence of Pacific SST forcing and planetary wave pattern on the North America warm season precipitation and heat waves (e.g., Castro et al. 2007a,b; Ciancarelli et al. 2014; Ding et al. 2011; Teng et al. 2013; Zhao et al. 2018). It is now more commonly acknowledged that the western Pacific–North America (WPNA; Ciancarelli et al. 2014) teleconnection and the circumglobal teleconnection (CGT; Ding and Wang 2005) are the main large-scale atmospheric patterns that modulate the precipitation and surface air temperature over North America. Ciancarelli et al. (2014) found that the well-known out-of-phase relationship between the central United States and Southwest summertime precipitation, which explained ~25% of the summer precipitation variability over the continental United States (CONUS), can be strongly influenced by the WPNA wave train, which is likely forced by Pacific SSTA in early summer [June–July (JJ)] and Indian monsoon convection in later summer [August–September (AS)]. The CGT pattern, on the other hand, is more related to the south-central and eastern U.S. precipitation and may be independent of Pacific SST forcing. The role of SSTA as a main driver of precipitation variability over the Great Plains has been further challenged by numerous studies arguing that the atmospheric internal variability and land–atmosphere feedbacks are the dominant drivers of the Great Plains summer drought for both short (Fernando et al. 2016; Hoerling et al. 2013; Pu et al. 2016; Wang et al. 2014) and long-term (Schubert et al. 2004) time scales. The modeling study of Ferguson et al. (2010) revealed that SST variability has no significant influence on drought frequency, duration, and magnitude outside the tropics, and that severe long-term droughts can occur over mid- and high-latitude regions in the absence of SSTA forcing. Correspondingly, the drought of 2012, the most severe drought over the central Great Plains since 1895, was also attributed to atmospheric variability with no significant contribution from SSTA forcing (Hoerling et al. 2014; Wang et al. 2014). Similar conclusions were made for the relative contribution of the SSTA and random atmospheric variability to the extreme drought of 2011 over Texas (Fernando et al. 2016; Seager et al. 2014; Wang et al. 2014).

One main source of potential predictability for summer droughts are the land–atmospheric feedbacks (e.g., Dirmeyer 1994; Hong and Kalnay 2000; Karl 1983; Myoung and Nielsen-Gammon 2010; Oglesby 1991; Oglesby and Erickson 1989; Rind 1982; Schubert et al. 2004; Zhuang et al. 2020), though most of these studies focus on local land–atmospheric feedbacks. Recently, numerical model experiments have shown remote land impacts on atmospheric circulation (e.g., Koster et al. 2016). Erfanian and Fu (2019) have evaluated the moisture budget over the Great Plains and found that anomalously dry moisture advection in spring was the main contributor to the onset of the summer extreme droughts over the Great Plains in 2011 and 2012. They hypothesized that such an anomalous dry advection was mainly due to the dryness of the land surface and lower troposphere over the U.S. Southwest in spring. Given the influence of ENSO on the Southwest dryness during winter and spring (e.g., Cook et al. 2011; Mo et al. 2009; Seager et al. 2008; Wang and Kumar 2015), we further hypothesize that the Southwest dryness can act as a springboard for Pacific SSTA and that the resultant large-scale atmospheric variability in cold season influences summer rainfall over the Great Plains. To evaluate these hypotheses in this study, we investigate whether there is a statistically significant relationship between antecedent precipitation and soil moisture in the Southwest in spring and subsequent summer precipitation in the Great Plains, and if so, whether this relationship from the spring through the summer is attributable to land surface feedback or to the evolution of large-scale atmospheric circulation responses associated with Pacific SSTs. We will also explore the potential predictability provided by this hypothesized remote land surface feedback mechanism by comparing the predictive skill for the Great Plains summer precipitation provided by this mechanism to that provided by the previous identified WPNA wave train forced by Pacific SSTA in early summer, using simple linear regression models.

## 2. Data and methodology

### a. Data

We used the European Centre for Medium-Range Weather Forecasts (ECMWF) interim reanalysis (ERAI) (Dee et al. 2011) for the moisture budget analysis described in section 2c. The ERAI reanalysis provides 6-hourly upper-air parameters from 1979 to near-real-time and its data are available online (http://apps.ecmwf.int/datasets/data/interim-full-daily/levtype=sfc/). The atmospheric model has a hybrid sigma-pressure vertical coordinate system with 60 levels and a T255 spectral horizontal resolution (~79 km).

The National Centers for Environmental Prediction (NCEP) Climate Prediction Center (CPC) unified gauge-based analysis of daily precipitation over the CONUS was used as the precipitation observation reference. Those data have a 0.25° × 0.25° resolution over the CONUS and are available from 1948 to present. For SST, the NOAA Extended Reconstructed SST version 5 (ERSSTv5) is used in this study. ERSSTv5 data have a 2° × 2° resolution and cover the period from 1854 to

present. These two datasets are both provided by the National Oceanic and Atmospheric Administration (NOAA) Earth System Research Laboratory (ESRL), Physical Science Division (PSD), Boulder, Colorado, at https://www.esrl.noaa.gov/psd/.

For evapotranspiration (ET) and surface soil moisture, we used the Global Land Evaporation Amsterdam Model (GLEAM) product version 3.3a (Martens et al. 2017). The GLEAM v3 provides an estimation of terrestrial evapotranspiration and root-zone soil moisture from satellite-observed soil moisture, vegetation optical depth and snow-water equivalent, reanalysis air temperature and radiation, and a multisource precipitation product. The data are available from 1980 to 2018 and can be downloaded from the project website (https://www.gleam.eu/).

### b. *Definitions of the Great Plains and the Southwest*

The analyses in this study largely focus on the Great Plains and the Southwest regions. Many previous studies have often given their own definitions as to the spatial coverage of these two regions for various research purposes. For example, Erfanian and Fu (2019) used the region of 105°–95°W, 30°–39°N for the southern Great Plains and 105°–95°W, 39°–48°N for the northern Great Plains. A more traditionally recognized spatial coverage for the Great Plains is that of Shafer et al. (2014) which spans a large area west of the Mississippi River tallgrass prairie and east of the Rocky Mountains. Here we use the region of 105°–95°W, 35°–47°N to represent the Great Plains as summer precipitation and spring zonal thermodynamic moisture advection are most correlated over this area so that it is suited for the research question in this study (as will be discussed in section 3a and Fig. 2a). For the Southwest, we use the region of 112°–105°W, 30°–43°N as spring precipitation over this region is most correlated with summer precipitation over the Great Plains (as will be discussed in section 3a and Fig. 2c). Note that the traditional definition for the Southwest usually just includes the states of Arizona and New Mexico, which only covers the southern part of the region defined here.

### c. *Atmospheric moisture budget*

To derive individual moisture tendencies, we used the water vapor budget equation for a unit mass of air (Yanai et al. 1973) as shown in Eq. (1):

$$\frac{\partial q}{\partial t} + \nabla \cdot (q\mathbf{v}) + \frac{\partial (q\omega)}{\partial p} = e - c, \tag{1}$$

where $t$, $q$, and $p$ stand for time, specific humidity, and pressure, respectively; $\mathbf{v}$ and $\omega$ are the horizontal wind vector and vertical wind velocity in pressure coordinates; and $e$ and $c$ are the evapotranspiration and condensation rates of the air parcel per unit mass, respectively.

Separating an arbitrary variable $A$ into a stationary $\tilde{A}$ and a transient contribution $\dot{A}$ ($A = \tilde{A} + \dot{A}$), implementing the covariance equation ($\widetilde{q\mathbf{v}} = \tilde{q}\tilde{\mathbf{v}} + \widetilde{\dot{q}\dot{\mathbf{v}}}$), and integrating it vertically from $P_t = 0$ to $P_s$, the moisture budget equation can be rearranged as the following:

$$\begin{aligned} &-\int_0^{P_s} \tilde{u}\partial_x\tilde{q}\,dp - \int_0^{P_s} \tilde{v}\partial_y\tilde{q}\,dp - \int_0^{P_s} \tilde{\omega}\frac{\partial\tilde{q}}{\partial p}dp \\ &-\int_0^{P_s}\left(\partial_x\widetilde{\dot{q}\dot{u}} + \partial_y\widetilde{\dot{q}\dot{v}} + \frac{\partial\widetilde{\dot{q}\dot{\omega}}}{\partial p}\right)dp = g\rho_w(P-E), \end{aligned} \tag{2}$$

where $u$ and $v$ are the zonal and meridional components of the horizontal wind $\mathbf{v}$. Here, the first three integrals on the left-hand side (LHS) represent the mean zonal, meridional, and vertical advection, respectively, and the last term represents the eddy transient terms for all three advections. The stationary and transient terms were calculated for the monthly mean and 6-hourly departure from the monthly mean, respectively. On the right-hand side (RHS), $P$ and $E$ are precipitation and evapotranspiration (ET) rates at the surface, and $g$ and $\rho_w$ stand for gravitational acceleration of Earth and water density.

Similar to the breakdown of variable $A$ into a stationary and a transient term, we separate the individual terms in Eq. (2) into a climatological mean and a monthly departure from climatology (e.g., $\tilde{A} = \overline{A} + A'$). The anomalous form of moisture budget equation can be rewritten as the following:

$$\begin{aligned} P' = &-\frac{1}{g\rho_w}\int_0^{P_s}(\overline{u}\partial_x q' + u'\partial_x\overline{q} + u'\partial_x q')\,dp \\ &-\frac{1}{g\rho_w}\int_0^{P_s}(\overline{v}\partial_y q' + v'\partial_y\overline{q} + v'\partial_y q')\,dp \\ &-\frac{1}{g\rho_w}\int_0^{P_s}\left(\overline{\omega}\frac{\partial q'}{\partial p} + \omega'\frac{\partial\overline{q}}{\partial p} + \omega'\frac{\partial q'}{\partial p}\right)dp + E' + \varepsilon', \end{aligned} \tag{3}$$

where $\varepsilon'$ is the residual term that accounts for the submonthly transient eddy contribution.

More details about the derivation of Eqs. (2) and (3) can be found in Erfanian and Fu (2019). The reanalysis parameters at the pressure levels below the surface are set to "missing values," and the horizontal and vertical gradients shown in Eqs. (2) and (3) were calculated using the "centered finite difference" function in NCAR Command Language (NCL). The individual moisture advection terms in both equations were calculated using 6-hourly ERAI reanalysis on a regular 0.75° grid and at 14 selected pressure levels. The vertical levels span from 1000 to 50 hPa with a resolution of 25 hPa for the lowest six levels (from 1000 to 850 hPa), which contain most of the atmospheric moisture, and relatively coarser resolutions of 50 and 100 hPa for the remaining levels in the middle and upper troposphere. The vertical integrals were calculated by multiplying the moisture tendencies in each layer by the pressure thickness of that layer ($dP$) and integrating the product from the surface to the 50-hPa level. The accuracy of the numerical calculations of moisture budget terms was evaluated against the ERAI reported vertically averaged moisture convergence in the work of Erfanian and Fu (2019). To ensure that the results were not sensitive to the choice of the reanalysis product, the same moisture budget analysis was repeated (Erfanian and Fu 2019) using the Modern-Era Retrospective Analysis for Research and Applications version 2 (MERRA-2) (Gelaro et al. 2017) and the results indicated a robust consistency between the two reanalyses.

*d. Linear regression modeling*

Over a sufficiently large area, precipitation anomalies on the LHS of Eq. (3) are balanced by a linear combination of anomalous tendency terms on the RHS. For use in the next section, to quantify the relative importance of individual tendency terms in estimating the summer precipitation over the Great Plains, the statistical model we adopt here is based on multiple linear regression, where the predictand is modeled as a linear combination of the predictors [RHS terms of Eq. (3) except the residual term $\varepsilon'$]. The general format of the multiple regression model is

$$P(i,j,t) = b_0(i,j) + \sum_{k=1}^{n} b_k(i,j)X_k(i,j,t). \quad (4)$$

Here $P(i, j, t)$ represents the standardized anomalies of seasonal [e.g., June–August (JJA)] precipitation spatially averaged over a 10° × 10° box centered at the grid cell $(i, j)$; $X_k(i, j, t)$ is the standardized anomaly of any term from the RHS of Eq. (3) spatially averaged over the same 10° × 10° box centered at the grid cell $(i, j)$ and $k$ varies from 1 to $n = 10$; $b_k(i, j)$ is the spatially varying regression coefficient determining the sensitivity of precipitation to $X_k(i, j, t)$ for each grid cell and $b_0(i, j)$ is a constant. The monthly standardized anomalies of both rainfall and moisture tendency terms were derived by first subtracting the climatological annual cycle from the monthly data, and then dividing the results by the standard deviation of each month. All regression coefficients were calculated by least squares fitting of the predictand and predictor time series for the 1992–2017 period. This period was selected for the regression analysis to avoid the impact of the artificial trend in the time series of ERAI moisture budget terms introduced by the abrupt changes in the Special Sensor Microwave Imager (SSM/I) observations and the retrieval of total column water vapor in 1992 (Trenberth et al. 2011).

Traditional multiple linear regression models determine regression coefficients by minimizing the loss function, which is the sum of the squares of the residuals made in the results of Eq. (4) (least squares). However, this is not the most suitable approach for our application here because we have a relatively small sample size compared to the number of predictors and too many predictors will lead to overfitting, and also some of the predictors may be correlated. To reduce multicollinearity, we use the least absolute shrinkage and selection operator (LASSO) regularization to perform variable selection. The LASSO approach can force the regression coefficients of some ''not so important'' predictors to become zero through adding an L1 penalty term ($\lambda\sum_{k=1}^{n}|b_k|$) to the loss function. In this study, we simply use LASSO to reduce predictor number and then perform traditional multiple regression with the selected predictors. This post-LASSO technique was shown to perform at least similarly as the LASSO regression in terms of convergence rate, and can achieve a smaller bias (Belloni and Chernozhukov 2013). Maximum number of predictors is set to be five. The regularization coefficient $\lambda$ in the L1 penalty term controls the amount of coefficient shrinkage and various values of $\lambda$ are used to construct LASSO regression models; larger $\lambda$ means more regularization and results in fewer nonzero regression coefficients. A fivefold cross validation is applied to estimate the mean squared error (MSE) for each regression model with a specific $\lambda$ value. For the one with minimum MSE, its predictors with nonzero regression coefficients will be selected for the final regression model without the penalty term.

The $R^2$ and $p$ value of the post-LASSO regression model are used to assess the model performance: i.e., how much of predictand variance can be explained by the selected predictors and is the model statistically significant. The regression coefficients $b_k$ will also be compared to determine the relative contribution of the selected predictors.

*e. Empirical orthogonal function analysis*

Empirical orthogonal function (EOF) analysis has been a widely used approach to extract individual modes of variability from data with complex spatial–temporal structures. We perform an EOF analysis to determine the dominant spatial pattern of midtropospheric circulation with 2-month or 3-month moving average monthly Z500 data during 1979–2017 from the ERAI. Rotated EOF (REOF) is a technique adopted since the mid-1980s (Richman 1986) to overcome some shortcomings of traditional EOF, e.g., difficulty of physical interpretability. The most well-known Varimax rotation method (Kaiser 1958; Richman 1986) is used for REOF, which is an orthogonal method, and the first five EOFs are chosen for rotation as the dominant REOF modes are relatively insensitive to a larger number of retained modes. Traditional EOF and REOF are both performed to determine which is more appropriate as to reflect the documented physical modes of climate variability, as will be shown in section 3b. Principal component time series for each EOF mode (PC) or for each REOF mode (RPC) are used for further correlation and regression analyses. Two spatial domains of input data will be used for different purposes: one smaller domain (180°–20°W, 20°–80°N) for identifying dominant modes of seasonal circulation variability most related to the North America region, and the other larger domain (120°E–20°W, 20°–80°N) to capture the summer WPNA wave train pattern.

*f. Correlation map and its significance*

We perform Pearson's correlation analysis between an area average variable $A(t)$ (e.g., JJA precipitation averaged over the Southwest) and a field variable $B(i, j, t)$ (e.g., seasonal precipitation, ET, SST). The field variable $B(i, j, t)$ is spatially averaged over a 10° × 10° box centered at the grid cell $(i, j)$ before the calculation of correlation coefficient. The significance of correlation coefficient $r$ is determined using a two-tailed Student's $t$ test with $N - 2$ degrees of freedom. Correlations with a $p$ value smaller than 0.05 will be considered statistically significant.

## 3. Results

*a. Relationship between summer precipitation over the Great Plains, spring zonal moisture advection, and dryness over the Southwest*

Summer is the major rainy season over the Great Plains with more than 40% of the annual rainfall occurring during JJA. According to the monthly climatology of 1979–2017, the

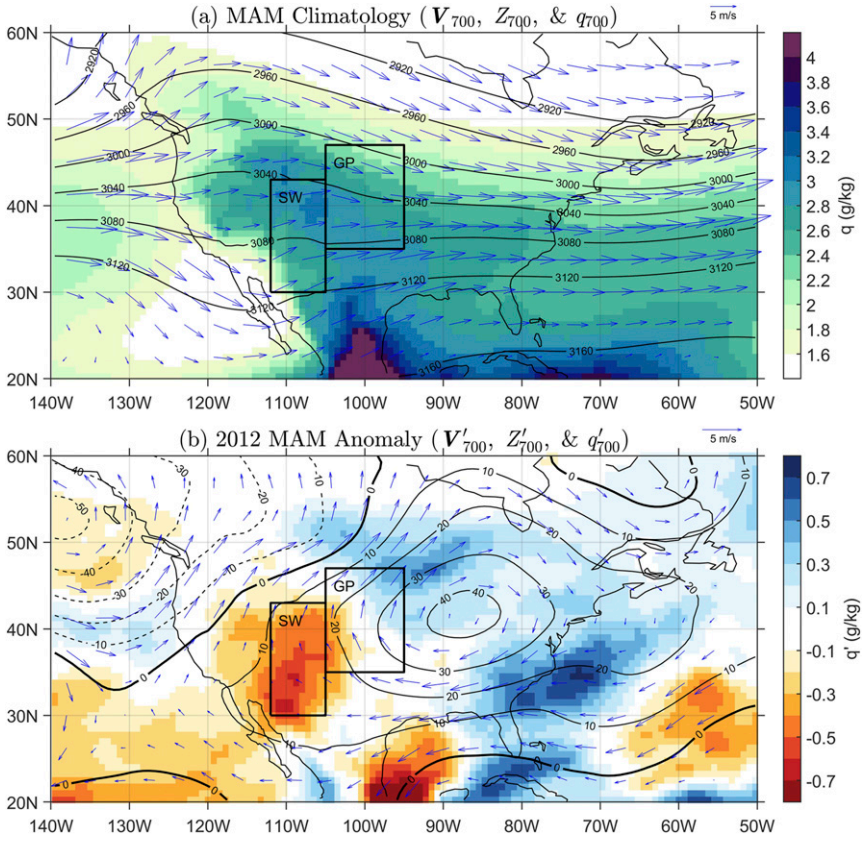


FIG. 1. (a) The MAM climatology (1979–2017) and (b) the 2012 MAM anomaly fields of 700-hPa specific humidity (g kg$^{-1}$; color shading), geopotential height (gpm; contours), and wind vectors from ERAI.

precipitation over the Great Plains increases from below 1 mm day$^{-1}$ in winter to near 3 mm day$^{-1}$ in late spring and early summer (Figs. S1a,d in the online supplemental material). Our moisture budget analysis over the Great Plains region (Fig. S2) shows that, among all the moisture tendency terms, the zonal advection tendency (ADV$_x$) is the dominant term of moisture flux convergence (MFC) above ~800 hPa over the region year round, while the meridional advection term (ADV$_y$) is dominant below ~800 hPa during late spring to early fall. The horizontal transient term (TRS$_h$) is the main contributor to moisture convergence from midfall to midspring when frontal systems occur frequently, but has negative values (moisture divergence) throughout the column during other times of the year. Overall, comparison of vertical integrals of these terms (third column of Fig. S2) and evapotranspiration (Figs. S1b,e) show that, although ADV$_x$ is not the top contributor in terms of amplitude during spring to early summer (i.e., it is smaller than evapotranspiration), it is the dominant term for the MFC and has the largest variation among all terms including evapotranspiration and is thus an important contributor for a moisture anomaly. A large departure of zonal advection from its climatological mean can result in substantial anomalies in the total MFC and thus precipitation over the region. Erfanian and Fu (2019) first confirmed this relationship and showed that the negative ADV$_x$ in spring sets the stage for summer droughts in 2011 and 2012. By definition, the zonal moisture advection term ADV$_x$ is the product of the zonal wind and zonal gradient of $q_v$. Figure 1 shows the March–May (MAM) climatology (1979–2017) of geopotential height, specific humidity, and wind field at 700 hPa ($Z_{700}$, $q_{700}$, and $\mathbf{V}_{700}$) over the North America and their 2012 MAM anomaly. As indicated by the $\mathbf{V}_{700}$ in Fig. 1a, strong westerlies prevail (that persist year around) over the entire North American continent. The MAM climatological mean of $q_{700}$ reveals a zonal gradient with higher $q_{700}$ values over the Rockies gradually decreasing moving toward the Great Plains and Midwest. The larger $q_{700}$ over the Rockies is likely because the high elevation of the Rockies places the surface level deep into the lower troposphere (700 hPa) and thus it can draw moisture from evapotranspiration of winter and spring precipitation more efficiently. At these levels, the zonal advection tendency becomes much larger than the meridional advection mainly due to the larger zonal wind speed (and near zero meridional wind). However, the zonal gradient of moisture is small and a strong decline of $q_{700}$ over the Great Plains' upwind region can change the direction of the climatological west–east moisture gradient and reverse the zonal advection from its largely positive climatology to negative anomalies

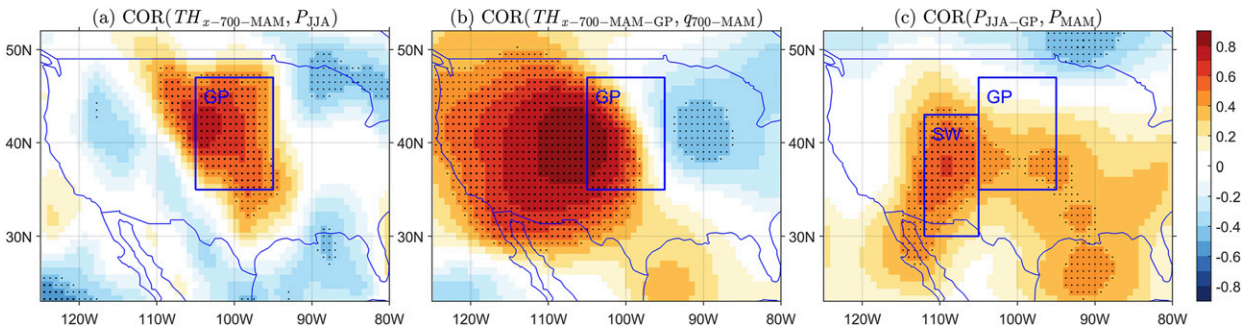


FIG. 2. Correlation maps between the standardized anomalous time series (1992–2017) of (a) the MAM zonal thermodynamic advection at 700 hPa ($TH_{x\text{-}700\text{-}MAM}$) and JJA precipitation ($P_{JJA}$) at each grid; (b) $TH_{x\text{-}700\text{-}MAM}$ averaged over the Great Plains ($TH_{x\text{-}700\text{-}MAM\text{-}GP}$) and MAM specific humidity at 700 hPa ($q_{700\text{-}MAM}$) at each grid; and (c) $P_{JJA}$ averaged over the Great Plains ($P_{JJA\text{-}GP}$) and MAM precipitation ($P_{MAM}$) at each grid. Grid points with correlation significant at the 0.05 level are marked with dots.

as large as those observed in the spring before the 2012 extreme drought (Fig. 1b).

Figure 2 shows the correlation between 700-hPa zonal thermodynamic advection ($TH_{x\text{-}700}$), specific humidity ($q_{700}$), and precipitation ($P$) during spring (MAM) and summer (JJA) based on ERAI data for the period of 1992–2017. In Fig. 2a, summertime precipitation ($P_{JJA}$) is significantly correlated to the springtime zonal thermodynamic term ($TH_{x\text{-}700\text{-}MAM}$) over the area of 105°–95°W, 35°–47°N. Because of its approximate overlap with the U.S. Great Plains region, we define the spatial coverage of the ''Great Plains'' (delineated in blue rectangle in Fig. 2a) as previously stated in section 2b. Figure 2b further shows that this $TH_{x\text{-}700\text{-}MAM}$ term averaged over the Great Plains ($TH_{x\text{-}700\text{-}MAM\text{-}GP}$) are positively correlated with specific humidity ($q_{700\text{-}MAM}$) in a vast region west of the Great Plains, with the largest correlation coefficient over 0.8, suggesting that low-level moisture variability over the upwind region of the Great Plains is a main contributor to the low-level zonal thermodynamic advection over the Great Plains in spring. In addition, to explore whether the summer precipitation over the Great Plains can be related to local or remote precipitation condition in antecedent spring, we evaluate the correlation between JJA rainfall anomalies averaged over the Great Plains ($P_{JJA\text{-}GP}$) and MAM rainfall anomalies over the CONUS (Fig. 2c). MAM rainfall anomalies over the Southwest domain show the highest correlation with the JJA rainfall anomalies over the Great Plains (mostly 0.5–0.7). The JJA rainfall anomalies over the Great Plains show less correlation (from 0 to 0.4) with the local MAM rainfall anomalies. The Southwest region shown in the blue rectangle is defined based on the largest correlation coefficients shown in Fig. 2c, and differs somewhat from the area commonly referred to as the ''Southwest.''

How do rainfall anomalies over the Southwest domain in spring (MAM) and late winter (January–March; JFM) influence lower tropospheric moisture anomalies ($q_{700\text{-}MAM}$) in the upwind region and the thermodynamic zonal moisture transport to the Great Plains in MAM ($TH_{x\text{-}700\text{-}MAM}$)? Fig. 3 shows a strong correlation between the lower tropospheric moisture anomalies in MAM and local evapotranspiration anomalies in MAM (Fig. 3a) and JFM (Fig. 3c), respectively, over the Southwest domain. The lower tropospheric moisture anomalies are also correlated with soil moisture anomalies in MAM (Fig. 3b), and JFM (Fig. 3d), respectively. The weaker correlation with soil moisture than with evapotranspiration is presumably because soil moisture varies more slowly than specific humidity does. Additional analysis shows that anomalies of evapotranspiration over the Southwest domain during drought years of the Great Plains were much stronger than that of the MFC, which was close to zero in spring and significantly negative throughout summer and early fall (Fig. S3). Evapotranspiration also has larger variability (standard deviation) than the MFC as well as other terms in the moisture budget equation [Eq. (3)] over the Southwest domain (Fig. S4). Figure 3, together with these additional analyses in Figs. S3 and S4, suggest that the lower tropospheric moisture anomalies over the upwind region of the Great Plains, especially over the Southwest, are mainly influenced by local evapotranspiration and soil moisture anomalies induced by rainfall anomalies in MAM and JFM, respectively. Such lower tropospheric moisture anomalies, in turn, affect the zonal thermodynamic moisture transport to the Great Plains in MAM.

To further evaluate the relative importance and predictive memory of zonal thermodynamic advection relative to other atmospheric moisture tendencies for variability of the U.S. summer precipitation, we construct a post-LASSO linear regression model between JJA precipitation and the moisture tendency terms at various pressure levels (plus the evapotranspiration term). The regression result for 800 hPa is shown in Fig. 4. For the Great Plains region, the post-LASSO regression model can explain up to ~60% of precipitation variance over much of the Great Plains domain (Fig. 4b). The relative importance of different terms can be compared with their corresponding regression coefficients. Figure 4 only shows the coefficient for the zonal thermodynamic advection term ($TH_x$; Fig. 4a), because the comparison between regression coefficients of all terms in the moisture budget equation (Figs. S5a–j) reveals the dominant contribution of this term over the Great Plains. In fact, a simpler regression model with only $TH_x$ as the predictor can explain well over 35% of precipitation variance (Fig. 4c) compared to ~60% explained by all the moisture budget terms over the Great Plains (Fig. 4b). Regression coefficients for all the other moisture terms

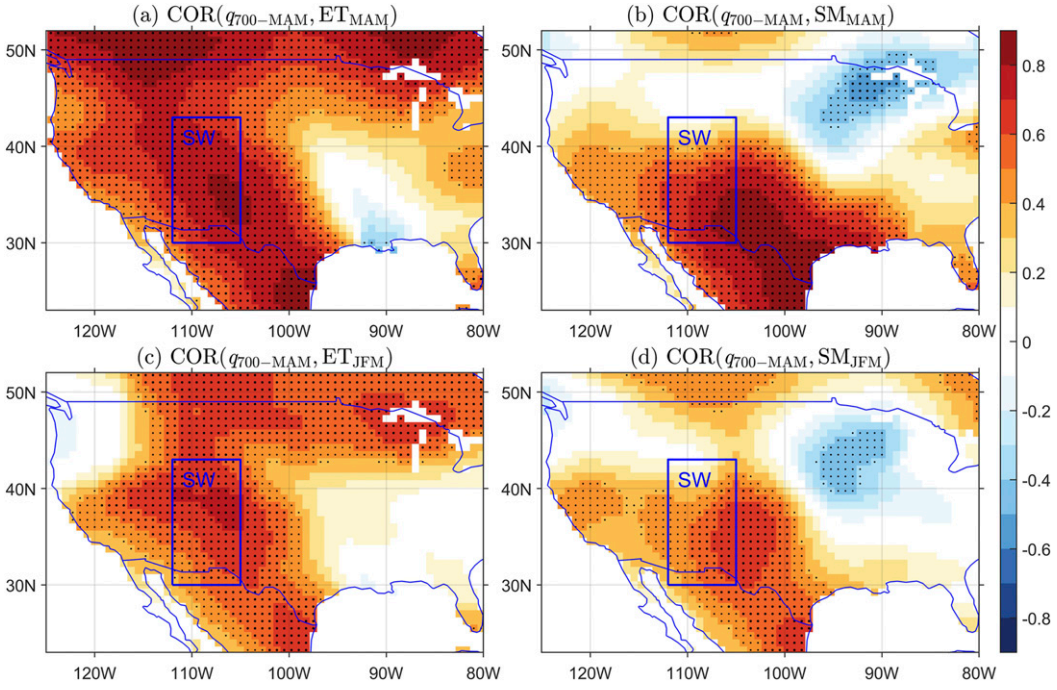


FIG. 3. Maps of local correlation between the time series (1992–2017) of the MAM specific humidity at 700 hPa ($q_{700\text{-MAM}}$) and the (a) MAM evapotranspiration (ET); (b) MAM surface soil moisture (SM); (c) JFM ET; and (d) JFM SM. Grid points with correlation significant at the 0.05 level are marked with dots.

indicate that the other two zonal advection terms (dynamic term $DN_x$ and nonlinear term $NL_x$) as well as the meridional nonlinear term ($NL_y$) play a secondary role as they have more points with near zero coefficients (Figs. S5b,c,f). This analysis indicates that the circulation anomalies have less influence on the anomalous zonal moisture advection in spring than the moisture gradient anomalies that are due to the drier surface of the Southwest. Other advection terms do not have a significant influence on JJA precipitation. Similar regression analysis on other pressure levels show that the dominant role of zonal thermodynamic advection term holds from 700 to 900 hPa (not shown), but is most prominent at 800–850 hPa.

How does moisture transport anomalies in spring affect rainfall in summer over the Great Plains? Could the anomalous thermodynamic moisture transport persist from spring to summer and directly influence the moisture budget and rainfall in JJA over the Great Plains? Fig. 5 shows the evolution of the correlation between JJA rainfall over the Great Plains ($P_{\text{JJA-GP}}$), and 3-month running means of the zonal thermodynamic moisture transport to that region ($TH_{x\text{-GP}}$, Fig. 5a), the specific humidity anomalies over the Great Plains ($q_{GP}$, Fig. 5b), and precipitation, evapotranspiration and soil moisture (Fig. 5c), respectively, from DJF to JJA. The significant correlation between JJA rainfall over the Great Plains and the zonal

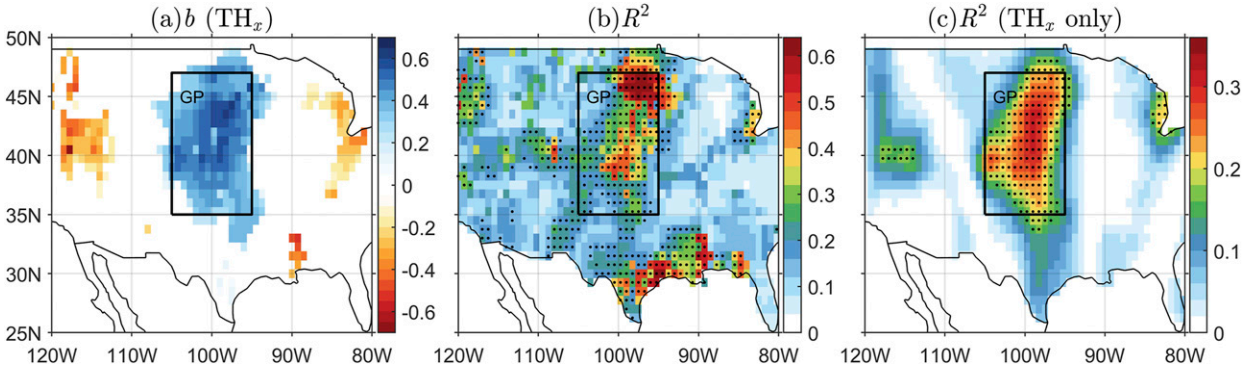


FIG. 4. Post-LASSO regression analysis with MAM moisture terms as predictors and local JJA precipitation as predictand (1992–2017). (a) Regression coefficients for zonal thermodynamic advection term ($TH_x$). (b) Coefficient of determination ($R^2$) for the post-LASSO regression model. (c) The $R^2$ statistic for a simple regression model with $TH_x$ as the sole predictor. Grid points with correlation significant at the 0.05 level are marked with dots.

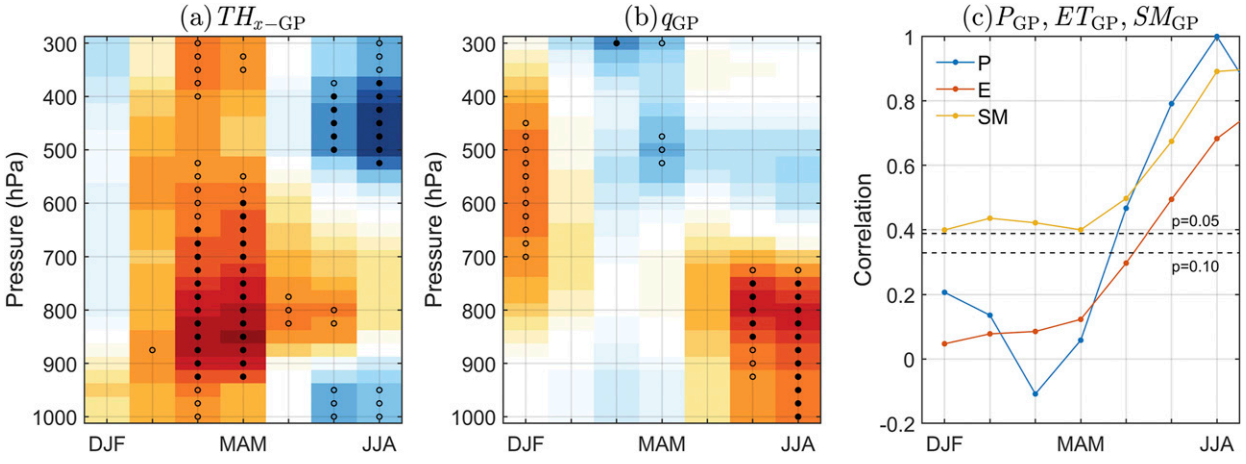


FIG. 5. Correlation between the standardized anomalous time series (1992–2017) of JJA precipitation averaged over the Great Plains ($P_{JJA\text{-}GP}$) and (a) the zonal thermodynamic advection at different pressure levels averaged over the Great Plains ($TH_{x\text{-}GP}$); (b) specific humidity at different pressure levels averaged over the Great Plains ($q_{GP}$); (c) precipitation, evapotranspiration, and surface soil moisture averaged over the Great Plains ($P_{GP}$, $ET_{GP}$, and $SM_{GP}$) from winter (DJF) to summer (JJA). Grid points with correlation significant at the 0.05 (0.10) level are marked with solid (hollow) dots.

thermodynamic moisture transport to that region persists from JFM to MJJ with $p < 10\%$ or from FMA to MAM with $p < 5\%$ (Fig. 5a). The JJA rainfall over the Great Plains is not significantly correlated with local lower tropospheric moisture (Fig. 5b), evapotranspiration, and rainfall (Fig. 5c) until late spring. Its correlation with soil moisture is marginally significant during DJF to MAM, presumably because of stronger persistence (autocorrelation) of the soil moisture anomalies. During MJJ to JJA, the JJA rainfall over the Great Plains is instead significantly correlated with the local lower tropospheric moisture (below 700 hPa, Fig. 5b), evapotranspiration, soil moisture, and rainfall (Fig. 5c). Additional analysis of the local relationships between all the contributing terms to the moisture budget and rainfall in JJA over the CONUS (Fig. S6) shows that the rainfall anomalies are most correlated with the local evapotranspiration (Fig. S6j) and the vertical thermodynamic moisture transport (driven by the vertical moisture gradient, Fig. S6g), instead of the horizontal moisture advection terms. Thus, Fig. 5 and Figs. S5 and S6 together suggest that the zonal thermodynamic moisture transport in MAM mainly influence moisture and rainfall in spring and early summer (May–June) over the Great Plains. The rainfall anomalies in early summer, in turn, influence the surface wetness and evapotranspiration, and consequently the local lower tropospheric moisture and rainfall over the Great Plains through local land–atmospheric feedbacks.

The above discussed combined remote and local land–atmospheric interaction inferred from our empirical evidence is consistent with the processes that control rainfall variability during spring and summer over the Great Plains suggested in literature. In particular, the detailed moisture budget analysis by Erfanian and Fu (2019) has suggested that an anomalous dry zonal moisture advection in spring of 2011 and 2012 is responsible for reduced lower tropospheric humidity over the Great Plains during spring and early summer, and suppresses deep convection. Fernando et al. (2016) has shown that the spring dry anomalies can trigger a positive feedback between soil moisture and large-scale circulation pattern within the Great Plains in summer. This local land surface feedback process in summer is the primary contributor to summer droughts over the Great Plains.

In summary, a springtime low-level moisture condition of the Southwest domain affects summer precipitation over the Great Plains through influencing the zonal moisture advection. This low-level moisture anomaly is mostly determined by local evapotranspiration anomalies induced by soil moisture and precipitation anomalies instead of by moisture transported from the Pacific. The remote land surface influence on moisture gradient in the lower troposphere between the Southwest and Great Plains influences rainfall over the Great Plains in late spring and early summer, which in turn continues to influence summer rainfall through local land–atmospheric feedbacks over the Great Plains. Thus, the combined remote and local land–atmospheric feedbacks play an important role in linking spring dryness over the Southwest and summer rainfall deficit over the Great Plains.

### *b. Large-scale teleconnections and their links to precipitation in Southwest spring and Great Plains summer*

In this section, we evaluate whether the apparent linkage between the Great Plains springtime zonal thermodynamic advection and the spring dryness over the Southwest, and the Great Plains summer precipitation shown in previous section is a result of large-scale atmospheric circulation response to the Pacific SSTA, as well as the relative influence of the remote land surface feedback and the large-scale atmospheric circulation response to the SSTA on the summer rainfall anomalies over the Great Plains.

To determine the dominant circulation modes for the North America region, we perform a REOF analysis for the 3-month moving average Z500. The second REOF (REOF2) mode displayed as correlation shown in Fig. 6a explains about 14%

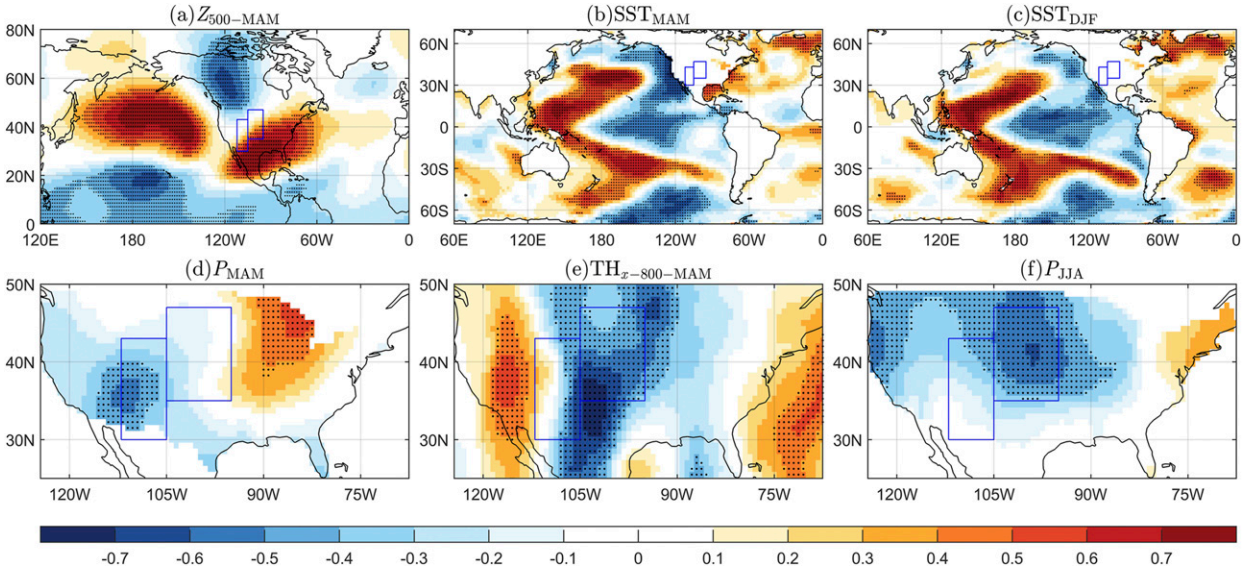


FIG. 6. Correlation maps between RPC2 in MAM and (a) Z500 in MAM; (b) SST in MAM; (c) SST in DJF; (d) precipitation in MAM; (e) zonal thermodynamic advection term at 800 hPa in MAM; (f) precipitation in JJA for the period of 1992–2017. Grid points with correlation significant at the 0.05 level are marked with dots.

of the variance. This wave-like pattern resembles the negative phase of PNA pattern in both spring and winter, with positive cells located over the southeastern United States and northern Pacific Ocean, and negative cells in the vicinity of Hawaii and western Canada (Wallace and Gutzler 1981). Correlations between the RPC2 in MAM and SST in both MAM and DJF (Figs. 6b,c), respectively, show that this mode is strongly associated with cold season Pacific SST variability (ENSO and PDO), as consistent with many previous studies (e.g., Wallace and Gutzler 1981). The correlations indicate an almost identical spatial pattern for both spring and winter SSTs with very weak correlations over the Atlantic and a cell of significant positive correlations over the central North Pacific surrounded by a horseshoe pattern of strongly negative correlations extending from the tropical Pacific (especially the Niño-3.4 region) to the northern and eastern Pacific and the western coast of the North America.

The RPC2 in MAM is further shown to be significantly correlated to precipitation over the Southwest (Fig. 6d) and the zonal thermodynamic advection downstream during MAM (Fig. 6e), and with the JJA precipitation over the Great Plains (Fig. 6f), possibly through the combined remote and local land–atmospheric coupling discussed in section 3a. Overall, these results suggest that during the cold season (from winter to spring), the Pacific SST conditions that resemble the cool phase of the PDO or the La Niña phase of the ENSO can lead to a negative phase of PNA-like circulation pattern, which favors a drier than normal spring over the Southwest and summer over the Great Plains, consistent with previous statistical and modeling studies (Hu and Huang 2009; McCabe et al. 2004; Schubert et al. 2009; Ting and Wang 1997). Complete results for the top five REOF are listed in Fig. S7, but none of them except the REOF2 mode is both associated with Pacific SST forcing and related to the Southwest spring precipitation.

Could the atmospheric circulation response to JJA Pacific SSTA forcing explain the summer precipitation over the Great Plains? Ciancarelli et al. (2014) identified the WPNA pattern associated with Pacific SST forcing as the dominant mode for precipitation variability over the central and northwestern United States in early summer. To test if this ENSO-related wave train circulation responses in early summer is responsible for rainfall variation over the Great Plains, we first perform an EOF analysis of the JJ Z500 (2-month mean) over the Pacific and North American domain as discussed in section 2e. The result of the second EOF (EOF2), which explains ~11% of the Z500 variance, is shown in Fig. 7a. Complete results of the EOF can be referred to Fig. S8. Here we only show the result for the EOF2 because it is most similar to the WPNA pattern identified in Ciancarelli et al. (2014). It shows a very clear quasi-stationary Rossby wave train originating from the western tropical Pacific (Fig. 7a). As expected, this ENSO-related circulation response pattern is significantly correlated to eastern tropical Pacific SST in early summer (Fig. 7b). However, correlation between its PC2 and precipitation in JJ reveals that this mode best explains the precipitation variability over the northwestern United States (Fig. 7c), and correlation over the northern part of the Great Plains is mostly less than 0.5, which translates to less than 25% of explained variance. This precipitation predictability provided by the JJ PC2 (representing WPNA pattern) is weaker that that provided by the previous MAM RPC2 (representing PNA-like pattern; Fig. 7d), where most of the Great Plains has the correlation up to 0.6 (36% of explained variance). Could the evolution of the PNA-like circulation associated with RPC2 from MAM to JJ cause the correlation between the lower tropospheric humidity and thermodynamic zonal moisture transport, respectively, in MAM and JJA rainfall over the Great Plains? We use the correlation map between the MAM RPC2 and JJ Z500

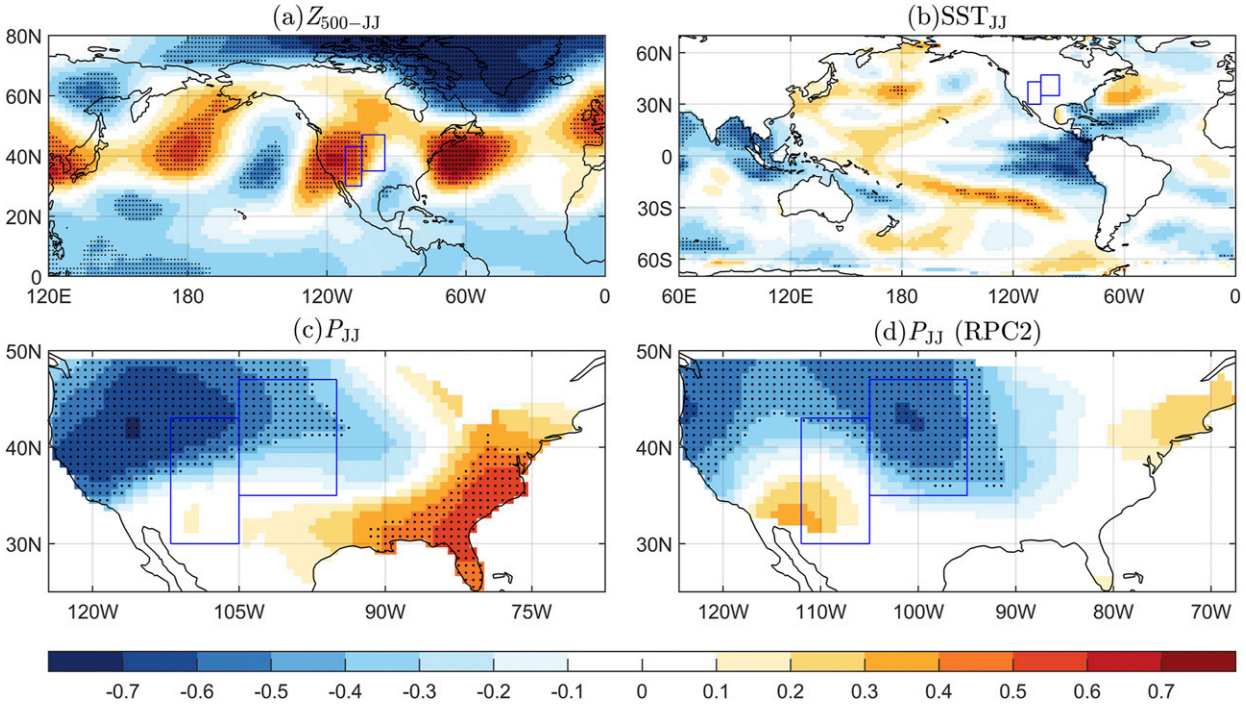


FIG. 7. Correlation maps between PC2 and (a) Z500 in JJ; (b) SST in JJ; (c) precipitation in JJ. (d) Correlation between RPC2 in MAM from Fig. 7 and precipitation in JJ. All correlation coefficients are calculated for the period of 1992–2017. Grid points with correlation significant at 0.05 level are marked with dots.

(Fig. S9) to represent such an evolution. This spatial pattern does not resemble those of the five leading EOF patterns for the JJ Z500 over the North Pacific–American–Atlantic sector, except for the EOF2 (Fig. S8, left column). Despite some resemblance between this JJ Z500 spatial pattern related to the MAM RPC2 (Fig. S9) and the WPNA (EOF2) pattern (Fig. 7a), the low temporal correlation (~0.15) between MAM RPC2 and JJ PC2 suggests that the WPNA in JJ is not evolved directly from the PNA-like pattern in MAM. Thus, the evolution of the large-scale circulation or the leading teleconnection patterns forced by Pacific SSTA from MAM to JJ cannot explain the observed temporal relationship between the lower tropospheric humidity and thermodynamic zonal moisture transport, respectively, in MAM and JJA rainfall over the Great Plains.

In summary, summer rainfall anomalies over the Great Plains are more correlated to a PNA-like teleconnection pattern (RPC2, Fig. 6) in spring than to the WPNA pattern in early summer (Fig. 7). Since the MAM PNA-like teleconnection is not significantly correlated with the leading EOF patterns of the JJ atmospheric circulation, the spring to summer evolution of large-scale atmospheric circulation pattern, and the major teleconnection patterns in summer such as WPNA pattern cannot explain the temporal correlation between the lower tropospheric humidity and thermodynamic zonal moisture transport, respectively, in MAM and JJA rainfall over the Great Plains. The latter seems to be best explained by the combined remote and local land–atmospheric coupling mechanism, i.e., the PNA-like circulation forced by Pacific SSTA in MAM induces anomalous rainfall and evapotranspiration over the Southwest in spring, leading to anomalous zonal moisture transport to the Great Plains. The latter, in turn, influences the atmospheric moisture budget, rainfall and soil moisture during May–June, during the onset of the summer rainy season dominated by tropical-like thermodynamic driven deep convection. These anomalies can initiate a local positive land–atmospheric feedbacks that can sustain and reinforce the rainfall anomalies through the rest of the summer season. Through such a chain of feedbacks, the rainfall anomalies over the Southwest induced by the Pacific SSTA in spring serves as a springboard for the cold season Pacific SSTA to influence warm season rainfall over the Great Plains.

## 4. Conclusions and discussion

Drought over the U.S. Great Plains is mainly contributed by its summer rainfall deficit. Our previous moisture budget analysis shows that the zonal advection dominates the moisture convergence year round, and a large negative departure from its climatology can lead to a strong precipitation deficit over the Great Plains (Erfanian and Fu 2019). We further showed that, for the 2011 and 2012 droughts over the Great Plains, a strong sensitivity of zonal thermodynamic advection to the west–east gradient of tropospheric moisture, facilitates a strong connection between the summer precipitation over the Great Plains and the atmospheric and land surface conditions over the upwind region, the Southwest and Rockies, during the antecedent spring.

This work explores the influences of rainfall anomalies over the Southwest and resulting changes of the zonal moisture

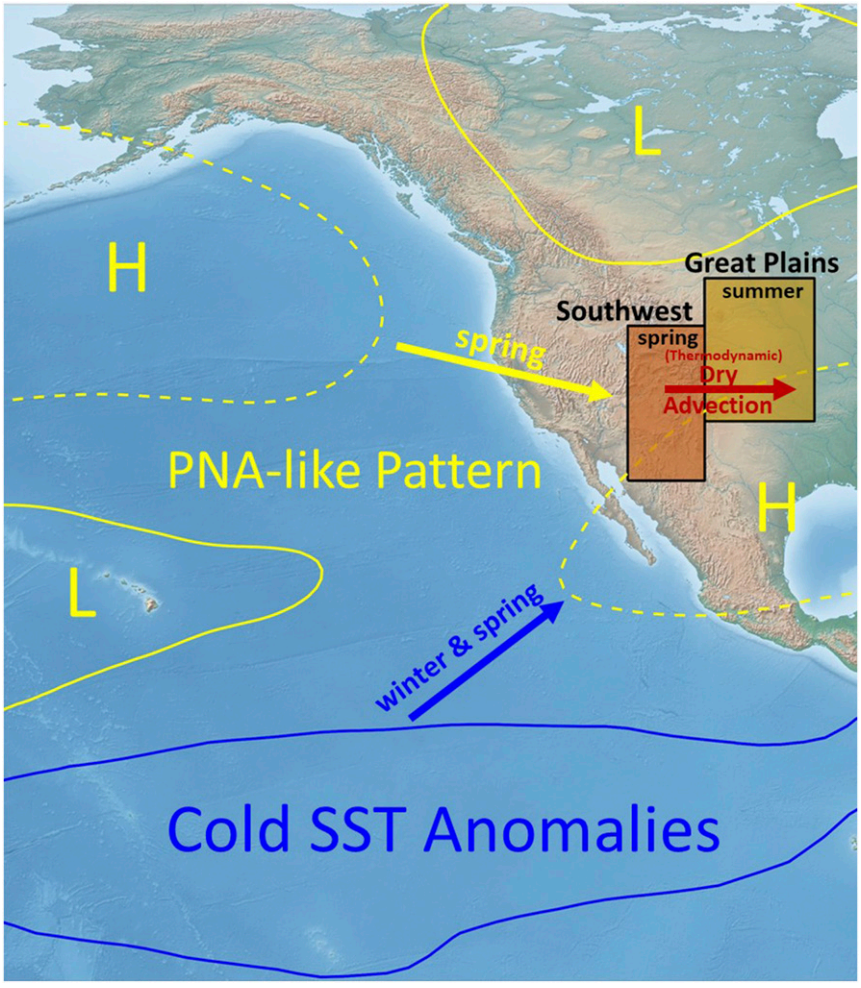


FIG. 8. The schematic illustration of the role of the Southwest as a springboard that links Pacific SST forcing in cold season to warm season precipitation anomalies over the Great Plains through the combined remote and local land–atmospheric feedbacks.

transport to the Great Plains on predictability of the summer rainfall anomalies over the Great Plains. Our correlation analysis and regression modeling reveal that the spring (MAM) zonal thermodynamic moisture advection anomaly in the lower troposphere is the most important term influencing the summer (JJA) precipitation over the Great Plains (Fig. 4), and that this term alone can explain over 35% of the total precipitation variance. This anomalous zonal moisture advection is mainly due to precipitation anomalies over the Southwest in spring, as well as soil moisture memory from winter to spring (Fig. 3). In contrast, the summer precipitation over the Great Plains shows near zero correlation with that in spring over the same region (Figs. 2c and 5c). While most of the previous studies in the literature have emphasized the local influence of land–atmospheric interaction on drought memory, our results suggests that the nonlocal land–atmospheric feedbacks are more important in determining the potential predictability of the summer precipitation over the Great Plains than are the local land–atmospheric feedbacks.

Our REOF analysis for Z500 shows that the variability of the Southwest rainfall and the zonal gradient of the tropospheric moisture between Southwest and the Great Plains in spring are correlated to the RPC2 time series of the REOF2 mode (Figs. 6d,e), a PNA-like teleconnection pattern (Fig. 6a), which is likely forced by anomalous cold season Pacific SST (Figs. 6b,c). Additionally, our analysis suggests that this PNA-like pattern in spring forced by Pacific SSTA (Figs. 6f and 7d), and resultant changes of the Southwest precipitation and the zonal thermodynamic moisture advection to the Great Plains in spring (Fig. 4c) explain a higher percentage of summer rainfall variance over the Great Plains than does a WPNA-like wave train in the early summer (Fig. 7c). This stronger influence of the spring teleconnection pattern on summer rainfall is a result of the remote land surface feedback mechanism identified in this study, especially through the influences of rainfall and evapotranspiration anomalies over the Southwest on moisture transport to the Great Plains.

Figure 8 provides a schematic illustration of how spring dryness over the Southwest serves as a springboard to connect

Pacific SST influences in winter and spring to the summer drought over the Great Plains: La Niña–like cold SST anomalies in winter and spring induce a negative phase PNA-like teleconnection pattern that results in rainfall deficits over the Southwest, which in turn change the moisture gradient between the Southwest and Great Plains in the lower troposphere, leading to anomalously dry zonal thermodynamic moisture advection in spring. This springtime zonal advection further influences the Great Plains precipitation in summer via the mechanism documented in Erfanian and Fu (2019). Thus, the time-lagged response of the Great Plains precipitation to that over the Southwest links the Great Plains summer precipitation to large-scale oceanic and atmospheric drivers in winter and spring. This mechanism could serve as a potential source for seasonal predictability of precipitation and so onset of extremely wet/dry summers over the Great Plains. Furthermore, given that future projections of global climate models indicate a more robust signal of intensified droughts over the Southwest as compared to the Great Plains (Cook et al. 2015; Feng et al. 2017; Hoerling et al. 2012; Ting et al. 2018), the relationship between the Southwest and Great Plains precipitation identified in this study implies an increased drought risk in summer for the Great Plains. At the very least, this mechanism will facilitate a better understanding of the outlook for Great Plains hydrologic extremes under future climate change scenarios.

Clearly, there are still uncertainties and unanswered open questions that require further investigation. For instance, this study, as well as Erfanian and Fu (2019), both show a strong connection between zonal moisture advection in spring and precipitation in summer over the Great Plains. We explained this interseasonal linkage via the influence of zonal moisture advection on the lower tropospheric humidity and convection entrainment, and the positive land surface feedback between precipitation and soil moisture. However, concrete evidence for validating this hypothesis is still absent and would require an analysis such as a moisture tracking model (e.g., Dominguez et al. 2006; Martinez and Dominguez 2014) to determine the source of Great Plains summer precipitation and more detailed process studies on the subseasonal scale to clarify the interaction between moisture transport, humidity profile, convection entrainment, surface soil moisture, and large-scale circulation. Additionally, as pointed out in section 2, there are abrupt changes in the SSM/I observations and the retrieval of total column water vapor in 1992, so only 26 seasonal samples (1992–2017) are used for most of our correlation and regression analysis. Therefore, caution is needed when interpreting the statistics from a regression analysis. Further research to verify the robustness of our conclusions across this study would require analyses using different reanalysis products over a longer time period.

*Acknowledgments.* The authors thank Robert E. Dickinson of University of California, Los Angeles, for his constructive input and comments on this research. This study was supported by funding from the National Oceanic and Atmospheric Climate Program Office (NOAA-CPO), Modeling, Analysis, Predictions, and Projections (MAPP) Program (NA17OAR4310123).

## REFERENCES

Anderson, W. B., R. Seager, W. Baethgen, M. Cane, and L. You, 2019: Synchronous crop failures and climate-forced production variability. *Sci. Adv.*, **5**, eaaw1976, https://doi.org/10.1126/SCIADV.AAW1976.

Belloni, A., and V. Chernozhukov, 2013: Least squares after model selection in high-dimensional sparse models. *Bernoulli*, **19**, 521–547, https://doi.org/10.3150/11-BEJ410.

Boyer, J. S., and Coauthors, 2013: The U.S. drought of 2012 in perspective: A call to action. *Global Food Secur.*, **2**, 139–143, https://doi.org/10.1016/j.gfs.2013.08.002.

Castro, C. L., R. A. Pielke, and J. O. Adegoke, 2007a: Investigation of the summer climate of the contiguous United States and Mexico using the Regional Atmospheric Modeling System (RAMS). Part I: Model climatology (1950–2002). *J. Climate*, **20**, 3844–3865, https://doi.org/10.1175/JCLI4211.1.

——, ——, ——, S. D. Schubert, and P. J. Pegion, 2007b: Investigation of the summer climate of the contiguous United States and Mexico using the regional atmospheric modeling system (RAMS). Part II: Model climate variability. *J. Climate*, **20**, 3866–3887, https://doi.org/10.1175/JCLI4212.1.

Chang, F. C., and J. M. Wallace, 1987: Meteorological conditions during heat waves and droughts in the United States Great Plains. *Mon. Wea. Rev.*, **115**, 1253–1269, https://doi.org/10.1175/1520-0493(1987)115<1253:MCDHWA>2.0.CO;2.

Chen, P., and M. Newman, 1998: Rossby wave propagation and the rapid development of upper-level anomalous anticyclones during the 1988 U.S. drought. *J. Climate*, **11**, 2491–2504, https://doi.org/10.1175/1520-0442(1998)011<2491:RWPATR>2.0.CO;2.

Ciancarelli, B., C. L. Castro, C. Woodhouse, F. Dominguez, H. I. Chang, C. Carrillo, and D. Griffin, 2014: Dominant patterns of US warm season precipitation variability in a fine resolution observational record, with focus on the southwest. *Int. J. Climatol.*, **34**, 687–707, https://doi.org/10.1002/joc.3716.

Cook, B. I., E. R. Cook, K. J. Anchukaitis, R. Seager, and R. L. Miller, 2011: Forced and unforced variability of twentieth century North American droughts and pluvials. *Climate Dyn.*, **37**, 1097–1110, https://doi.org/10.1007/s00382-010-0897-9.

——, T. R. Ault, and J. E. Smerdon, 2015: Unprecedented 21st century drought risk in the American Southwest and Central Plains. *Sci. Adv.*, **1**, e1400082, https://doi.org/10.1126/SCIADV.1400082.

Dee, D. P., and Coauthors, 2011: The ERA-Interim reanalysis: Configuration and performance of the data assimilation system. *Quart. J. Roy. Meteor. Soc.*, **137**, 553–597, https://doi.org/10.1002/qj.828.

Ding, Q. H., and B. Wang, 2005: Circumglobal teleconnection in the Northern Hemisphere summer. *J. Climate*, **18**, 3483–3505, https://doi.org/10.1175/JCLI3473.1.

——, ——, J. M. Wallace, and G. Branstator, 2011: Tropical-extratropical teleconnections in boreal summer: Observed interannual variability. *J. Climate*, **24**, 1878–1896, https://doi.org/10.1175/2011JCLI3621.1.

Dirmeyer, P. A., 1994: Vegetation stress as a feedback mechanism in midlatitude drought. *J. Climate*, **7**, 1463–1483, https://doi.org/10.1175/1520-0442(1994)007<1463:VSAAFM>2.0.CO;2.

Dominguez, F., P. Kumar, X. Z. Liang, and M. F. Ting, 2006: Impact of atmospheric moisture storage on precipitation recycling. *J. Climate*, **19**, 1513–1530, https://doi.org/10.1175/JCLI3691.1.

Erfanian, A., and R. Fu, 2019: The role of spring dry zonal advection in summer drought onset over the US Great Plains.

*Atmos. Chem. Phys.*, **19**, 15 199–15 216, https://doi.org/10.5194/acp-19-15199-2019.

Feng, S., Q. Hu, and R. J. Oglesby, 2011: Influence of Atlantic sea surface temperatures on persistent drought in North America. *Climate Dyn.*, **37**, 569–586, https://doi.org/10.1007/s00382-010-0835-x.

——, M. Trnka, M. Hayes, and Y. J. Zhang, 2017: Why do different drought indices show distinct future drought risk outcomes in the U.S. Great Plains? *J. Climate*, **30**, 265–278, https://doi.org/10.1175/JCLI-D-15-0590.1.

Ferguson, I. M., J. A. Dracup, P. B. Duffy, P. Pegion, and S. Schubert, 2010: Influence of SST forcing on stochastic characteristics of simulated precipitation and drought. *J. Hydrometeor.*, **11**, 754–769, https://doi.org/10.1175/2009JHM1132.1.

Fernando, D. N., and Coauthors, 2016: What caused the spring intensification and winter demise of the 2011 drought over Texas? *Climate Dyn.*, **47**, 3077–3090, https://doi.org/10.1007/s00382-016-3014-x.

Gelaro, R., and Coauthors, 2017: The Modern-Era Retrospective Analysis for Research and Applications, version 2 (MERRA-2). *J. Climate*, **30**, 5419–5454, https://doi.org/10.1175/JCLI-D-16-0758.1.

Hoerling, M. P., J. K. Eischeid, X. W. Quan, H. F. Diaz, R. S. Webb, R. M. Dole, and D. R. Easterling, 2012: Is a transition to semipermanent drought conditions imminent in the U.S. Great Plains? *J. Climate*, **25**, 8380–8386, https://doi.org/10.1175/JCLI-D-12-00449.1.

——, and Coauthors, 2013: An interpretation of the origins of the 2012 central Great Plains drought. NOAA Assessment Rep., 44 pp., https://psl.noaa.gov/csi/factsheets/pdf/noaa-gp-drought-assessment-report.pdf.

——, J. Eischeid, A. Kumar, R. Leung, A. Mariotti, K. Mo, S. Schubert, and R. Seager, 2014: Causes and predictability of the 2012 Great Plains drought. *Bull. Amer. Meteor. Soc.*, **95**, 269–282, https://doi.org/10.1175/BAMS-D-13-00055.1.

Hong, S. Y., and E. Kalnay, 2000: Role of sea surface temperature and soil-moisture feedback in the 1998 Oklahoma-Texas drought. *Nature*, **408**, 842–844, https://doi.org/10.1038/35048548.

Hu, Q., and S. Feng, 2008: Variation of the North American summer monsoon regimes and the Atlantic multidecadal oscillation. *J. Climate*, **21**, 2371–2383, https://doi.org/10.1175/2007JCLI2005.1.

Hu, Z. Z., and B. H. Huang, 2009: Interferential impact of ENSO and PDO on dry and wet conditions in the U.S. Great Plains. *J. Climate*, **22**, 6047–6065, https://doi.org/10.1175/2009JCLI2798.1.

Kaiser, H. F., 1958: The varimax criterion for analytic rotation in factor-analysis. *Psychometrika*, **23**, 187–200, https://doi.org/10.1007/BF02289233.

Karl, T. R., 1983: Some spatial characteristics of drought duration in the United-States. *J. Climate Appl. Meteor.*, **22**, 1356–1366, https://doi.org/10.1175/1520-0450(1983)022<1356:SSCODD>2.0.CO;2.

Koster, R. D., Y. H. Chang, H. L. Wang, and S. D. Schubert, 2016: Impacts of local soil moisture anomalies on the atmospheric circulation and on remote surface meteorological fields during boreal summer: A comprehensive analysis over North America. *J. Climate*, **29**, 7345–7364, https://doi.org/10.1175/JCLI-D-16-0192.1.

Lobell, D. B., M. J. Roberts, W. Schlenker, N. Braun, B. B. Little, R. M. Rejesus, and G. L. Hammer, 2014: Greater sensitivity to drought accompanies maize yield increase in the U.S. Midwest. *Science*, **344**, 516–519, https://doi.org/10.1126/science.1251423.

Lyon, B., and R. M. Dole, 1995: A diagnostic comparison of the 1980 and 1988 U.S. summer heat wave-droughts. *J. Climate*, **8**, 1658–1675, https://doi.org/10.1175/1520-0442(1995)008<1658:ADCOTA>2.0.CO;2.

Martens, B., and Coauthors, 2017: GLEAM v3: Satellite-based land evaporation and root-zone soil moisture. *Geosci. Model Dev.*, **10**, 1903–1925, https://doi.org/10.5194/gmd-10-1903-2017.

Martinez, J. A., and F. Dominguez, 2014: Sources of atmospheric moisture for the La Plata river basin. *J. Climate*, **27**, 6737–6753, https://doi.org/10.1175/JCLI-D-14-00022.1.

McCabe, G. J., M. A. Palecki, and J. L. Betancourt, 2004: Pacific and Atlantic Ocean influences on multidecadal drought frequency in the United States. *Proc. Natl. Acad. Sci. USA*, **101**, 4136–4141, https://doi.org/10.1073/pnas.0306738101.

Mo, K. C., J. K. E. Schemm, and S. H. Yoo, 2009: Influence of ENSO and the Atlantic multidecadal oscillation on drought over the United States. *J. Climate*, **22**, 5962–5982, https://doi.org/10.1175/2009JCLI2966.1.

Myoung, B., and J. W. Nielsen-Gammon, 2010: The convective instability pathway to warm season drought in Texas. Part I: The role of convective inhibition and its modulation by soil moisture. *J. Climate*, **23**, 4461–4473, https://doi.org/10.1175/2010JCLI2946.1.

Namias, J., 1991: Spring and summer 1988 drought over the contiguous United States—Causes and prediction. *J. Climate*, **4**, 54–65, https://doi.org/10.1175/1520-0442(1991)004<0054:SASDOT>2.0.CO;2.

Oglesby, R. J., 1991: Springtime soil-moisture, natural climatic variability, and North American drought as simulated by the NCAR Community Climate Model 1. *J. Climate*, **4**, 890–897, https://doi.org/10.1175/1520-0442(1991)004<0890:SSMNCV>2.0.CO;2.

——, and D. J. Erickson, 1989: Soil moisture and the persistence of North American drought. *J. Climate*, **2**, 1362–1380, https://doi.org/10.1175/1520-0442(1989)002<1362:SMATPO>2.0.CO;2.

Pu, B., R. Fu, R. E. Dickinson, and D. N. Fernando, 2016: Why do summer droughts in the Southern Great Plains occur in some La Nina years but not others? *J. Geophys. Res. Atmos.*, **121**, 1120–1137, https://doi.org/10.1002/2015JD023508.

Quan, X. W., M. P. Hoerling, B. Lyon, A. Kumar, M. A. Bell, M. K. Tippett, and H. Wang, 2012: Prospects for dynamical prediction of meteorological drought. *J. Appl. Meteor. Climatol.*, **51**, 1238–1252, https://doi.org/10.1175/JAMC-D-11-0194.1.

Richman, M. B., 1986: Rotation of principal components. *J. Climatol.*, **6**, 293–335, https://doi.org/10.1002/joc.3370060305.

Rind, D., 1982: The influence of ground moisture conditions in North America on summer climate as modeled in the GISS GCM. *Mon. Wea. Rev.*, **110**, 1487–1494, https://doi.org/10.1175/1520-0493(1982)110<1487:TIOGMC>2.0.CO;2.

Schubert, S. D., M. J. Suarez, P. J. Pegion, R. D. Koster, and J. T. Bacmeister, 2004: Causes of long-term drought in the US Great Plains. *J. Climate*, **17**, 485–503, https://doi.org/10.1175/1520-0442(2004)017<0485:COLDIT>2.0.CO;2.

——, and Coauthors, 2009: A U.S. CLIVAR project to assess and compare the responses of global climate models to drought-related SST forcing patterns: Overview and results. *J. Climate*, **22**, 5251–5272, https://doi.org/10.1175/2009JCLI3060.1.

Seager, R., and M. Hoerling, 2014: Atmosphere and ocean origins of North American droughts. *J. Climate*, **27**, 4581–4606, https://doi.org/10.1175/JCLI-D-13-00329.1.

——, R. Burgman, Y. Kushnir, A. Clement, E. Cook, N. Naik, and J. Miller, 2008: Tropical pacific forcing of North American

medieval megadroughts: Testing the concept with an atmosphere model forced by coral-reconstructed SSTs. *J. Climate*, **21**, 6175–6190, https://doi.org/10.1175/2008JCLI2170.1.

——, L. Goddard, J. Nakamura, N. Henderson, and D. E. Lee, 2014: Dynamical causes of the 2010/11 Texas–northern Mexico drought. *J. Hydrometeor.*, **15**, 39–68, https://doi.org/10.1175/JHM-D-13-024.1.

Shafer, M., and Coauthors, 2014: Great Plains. *Climate Change Impacts in the United States: The Third National Climate Assessment*, J. M. Melillo, T. C. Richmond, and G. W. Yohe, Eds., U.S. Global Change Research Program, 441–461.

Sutton, R. T., and D. L. R. Hodson, 2005: Atlantic Ocean forcing of North American and European summer climate. *Science*, **309**, 115–118, https://doi.org/10.1126/science.1109496.

Teng, H. Y., G. Branstator, H. L. Wang, G. A. Meehl, and W. M. Washington, 2013: Probability of US heat waves affected by a subseasonal planetary wave pattern. *Nat. Geosci.*, **6**, 1056–1061, https://doi.org/10.1038/ngeo1988.

Ting, M. F., and H. Wang, 1997: Summertime U.S. precipitation variability and its relation to Pacific sea surface temperature. *J. Climate*, **10**, 1853–1873, https://doi.org/10.1175/1520-0442(1997)010<1853:SUSPVA>2.0.CO;2.

——, R. Seager, C. H. Li, H. B. Liu, and N. Henderson, 2018: Mechanism of future spring drying in the southwestern United States in CMIP5 models. *J. Climate*, **31**, 4265–4279, https://doi.org/10.1175/JCLI-D-17-0574.1.

Trenberth, K. E., G. W. Branstator, and P. A. Arkin, 1988: Origins of the 1988 North American drought. *Science*, **242**, 1640–1645, https://doi.org/10.1126/science.242.4886.1640.

——, J. T. Fasullo, and J. Mackaro, 2011: Atmospheric moisture transports from ocean to land and global energy flows in reanalyses. *J. Climate*, **24**, 4907–4924, https://doi.org/10.1175/2011JCLI4171.1.

Wallace, J. M., and D. S. Gutzler, 1981: Teleconnections in the geopotential height field during the Northern Hemisphere winter. *Mon. Wea. Rev.*, **109**, 784–812, https://doi.org/10.1175/1520-0493(1981)109<0784:TITGHF>2.0.CO;2.

Wang, H., and A. Kumar, 2015: Assessing the impact of ENSO on drought in the U.S. Southwest with NCEP climate model simulations. *J. Hydrol.*, **526**, 30–41, https://doi.org/10.1016/j.jhydrol.2014.12.012.

Wang, H. L., S. Schubert, M. Suarez, and R. Koster, 2010: The physical mechanism by which the leading patterns of SST variability impact U.S. precipitation. *J. Climate*, **23**, 1815–1836, https://doi.org/10.1175/2009JCLI3188.1.

——, ——, R. Koster, Y. G. Ham, and M. Suarez, 2014: On the role of SST forcing in the 2011 and 2012 extreme U.S. Heat and drought: A study in contrasts. *J. Hydrometeor.*, **15**, 1255–1273, https://doi.org/10.1175/JHM-D-13-069.1.

Yanai, M., S. Esbensen, and J. H. Chu, 1973: Determination of bulk properties of tropical cloud clusters from large-scale heat and moisture budgets. *J. Atmos. Sci.*, **30**, 611–627, https://doi.org/10.1175/1520-0469(1973)030<0611:DOBPOT>2.0.CO;2.

Zhao, S., Y. Deng, and R. X. Black, 2018: An intraseasonal mode of atmospheric variability relevant to the US hydroclimate in boreal summer: Dynamic origin and East Asia connection. *J. Climate*, **31**, 9855–9868, https://doi.org/10.1175/JCLI-D-18-0206.1.

——, ——, and ——, 2017: Observed and simulated spring and summer dryness in the United States: The impact of the Pacific Sea surface temperature and beyond. *J. Geophys. Res. Atmos.*, **122**, 12 713–12 731, https://doi.org/10.1002/2017JD027279.

Zhuang, Y. Z., R. Fu, and H. Q. Wang, 2020: Large-scale Atmospheric circulation patterns associated with US Great Plains warm season droughts revealed by self-organizing maps. *J. Geophys. Res. Atmos.*, **125**, e2019JD031460, https://doi.org/10.1029/2019JD031460.